Aerodynamic Design of VTOL Micro Air Vehicles

Sergey Shkarayev[1]
The University of Arizona, Tucson, AZ, USA, 85721

Jean-Marc Moschetta[2] and Boris Bataille[3]
SUPAERO, Toulouse, France, 35055

The research and development efforts outlined in this paper address the aerodynamic design of micro air vehicles (MAVs) with hovering, vertical take-off, and landing capabilities (VTOL). The tilt-body configuration of the VTOL MAV is proposed based on the propulsion system consisting of two coaxial contra-rotating motors-propellers. Values of thrust, torque, power, and efficiency of this propulsion system were measured in pusher and tractor arrangements of propellers and compared against single motor-propeller propulsion. With comparable efficiency, the developed propulsion system has very little propeller torque. Hot-wire measurements have been conducted to investigate the velocity profile in slipstream. The lower average velocity and significant decrease of velocity in the core of the slipstream found in the tractor arrangement are mostly due to the parasite drag caused by the motors. It causes the decrease of the thrust force observed for the tractor arrangement in comparison with the pusher one. Wind tunnel testing was conducted for a motor, a wing, and an arrangement of a wing with a motor. The drag force on the wing is produced by two mixing airflows: free stream and propeller-induced pulsating slipstream. The zero-lift drag coefficient increases by about three times with propeller-induced speed increase from 0 to 15 m/s indicating the change of transition mechanism in the boundary layer from a laminar to turbulent state. The results of this study were realized in the design of a VTOL MAV prototype that was successfully flight tested.

Nomenclature

C_D	=	drag coefficient
C_{D_0}	=	zero-lift drag coefficient
C_L	=	lift coefficient
c	=	chord
F_{total}	=	total force measured by a wind tunnel balance
P	=	electric power input
P_{ind}	=	induced power
Q	=	torque
R	=	propeller radius
R_m	=	maximum distance of velocity measurements from the s-axis
Re	=	mean aerodynamic chord Reynolds number
S_0	=	wing area
S_p	=	area of a part of the wing covered by propeller slipstream
S_S	=	area of the side wall
T	=	thrust force
T_s	=	thrust force determined from air velocity data
V_0	=	free stream velocity

[1] Associate Professor, Aerospace and Mechanical Engineering Dept., 1130 N. Mountain Ave.
[2] Professor, Department of Aerodynamics, SUPAERO BP 54032.
[3] Research Assistant, Department of Aerodynamics, SUPAERO BP 54032.

W	=	take-off weight of an aircraft
$w(s)$	=	induced velocity based on propeller momentum theory
w_e	=	measured induced velocity
w_{ult}	=	ultimate propeller-induced velocity
α	=	angle of attack
ρ	=	air density

I. Introduction

THE truly successful use of MAV technology is somewhat difficult without the capability of aggressive vertical maneuvering and hovering autonomously. One way to fulfill these requirements is in the design of rotary wing MAVs, and several helicopters have been developed in recent years. However, they are sensitive to air turbulence due to their large rotor disc. In general, when compared to fixed-wing aircraft, rotorcrafts have a smaller range, endurance, and payload capacity.

Design methods and general theoretical aerodynamic principles for large VTOL aircraft are well developed and have been summarized in the literature.[1,2] As the field of VTOL evolved, much attention was paid to propulsion system considerations and development of an aerodynamic theory for the propeller and rotor. Other subjects included design studies of configurations and control issues during hover and transition. Overall, there is a sufficient amount of relevant data and knowledge to begin exploring the VTOL concept with applications to MAVs.

In the present study, we begin a research project on novel fixed-wing MAVs capable of vertical take-off and landing, and hovering, based upon our previous successful designs. The University of Arizona has developed one of the world's smallest mission-capable autonomous MAVs, the Dragonfly.[3] Obviously, adding hovering capabilities to these aircraft requires additional motor power to get off the ground without using the wings' aerodynamics. Another technical problem is in controlling the vehicle transition from vertical to horizontal flight. In order to provide effective control at low speed, the MAVs will feature large control surfaces and throws, changing the baseline design in a significant way. The present project will also benefit from an independent experimental study of the "Vertigo" concept developed at SUPAERO.[4] The Vertigo consists of a fixed delta wing powered by coaxial contra-rotating propellers and side by side motors. Its capability to hover and transition flights has been recently demonstrated on a radio-controlled prototype.

In the following discussion, the two concepts for VTOL MAVs will be briefly presented, and their aerodynamics, performance, and controls will be examined. The two concepts are (1) single propeller tilt-body aircraft and (2) contra-rotating propellers tilt-body aircraft.

Aerobatic single-propeller RC aircraft emerged as a result of the integration of the latest developments in electric motor and battery technology into a lightweight structure. With high thrust-to-weight ratio and large control surfaces and throws, these airplanes can perform spectacular aerobatic maneuvers. However, they feature a very low wing loading, resulting in a very low flight speed.

In general, designing of a single-propeller tilt-body MAV is largely affected by the following basic issues of the propulsion itself: propeller torque, p-factor, swirling slipstream, and gyroscopic moment. The propeller torque, which appears as a left rolling tendency, is a serious drawback in a single propeller-driven aircraft. Typically, the wingspan of aerobatic airplanes is greater than 1 m, which limits the maximum torque-roll rate by about 180º per second, allowing an inexperienced pilot to control the airplane. The maximum size for MAVs is 3-5 times smaller. Assuming that the torque-roll rate is inversely proportional to the square of the wing span, if the wingspan of an MAV decreases by a factor of 2, the torque-roll rate increases by a factor of 4. Thus, the torque-roll may become a driving factor in the design of the control system for VTOL MAVs.

Another negative effect in the single-propeller-driven aircraft is the p-factor that occurs as a result of the difference in angle of attack between the blades of a rotating propeller and causes a single-engine propeller aircraft to yaw to the left. Keeping the rudder to the right helps to maintain straight flight, however, as a consequence, the aircraft drag increases.

The effect of the rotational airflow is inherent to a single-propeller propulsion system. The air rotating into a twisting helix around the fuselage presses against the left side of the ventral vertical tail, causing the plane to yaw and roll to the left. It also results in energy losses, reducing overall thrust efficiency of the propulsion.

In a tilt-body VTOL with contra-rotating propellers, the second coaxial propeller is installed immediately behind the first one and rotates in the direction opposite to the rotating flow after the first one. The air flow coming out of contra-rotating propeller is symmetrical, without a torque and side forces. The induced velocity behind the first propeller may increase the total thrust of the system in comparison with two propellers staying apart.

In 1953-55, Convair designed and successfully tested the XFY-1 Pogo aircraft with contra-rotating propellers. Pogo has successfully completed VTOL flights, but the project was cancelled at completion of the test program. A jet tail-sitter, Ryan X-13 Vertijet, also completed VTOL flights in 1956-57. Historically, large tilt-body tail-sitters have been envisioned for military use on both land and sea in situations disallowing airfields, or for operating from limited space. Although short-lived, tail-sitters paved the way for fixed-wing, jet-thrust-vectored aircraft, such as the Harrier. Among the problems, the pilot's uncomfortable accommodation was an important one, which, of course, is not important for unmanned air vehicles. Therefore, the tail-sitter designs with contra-rotating propellers-motors are the focus of the current project.

Aerodynamic interaction of the wing with the propeller was studied by Prandtl[5] in a wind tunnel. In a series of tests, lift, drag, and pitching moment on the wing and propeller thrust were measured. Increase of the drag was found to be noticeable when the wing propeller is right behind the propeller. One of the issues of the interpretation of propeller-wing interaction is the right choice of reference speed. The increase of the speed behind the propeller was used[5] for the explanation of the effect of drag increase, however, only a free stream speed was employed as a reference speed in the drag coefficient calculations, thus, not taking into account actual propeller-induced velocity.

In general, a propeller generates a pulsating slipstream that can diminish the enhanced performance of laminar wings in a tractor configuration. On the other hand, a pure pusher configuration is not an acceptable solution for VTOL aircraft that employ a propeller slipstream in aerodynamic controls.

In an earlier work,[6] the laminar boundary layer was investigated on the NACA 27-212 airfoil in the presence of a free stream and propeller slipstream. It was found that the laminar-to-turbulent transition point is moving toward the leading edge of the wing, causing a significant increase in the drag.

One of applications of large unmanned air vehicles is for high-altitude surveillance. Aerodynamic design of this class of vehicles requires investigation of propeller-wing interaction at low Reynolds numbers, but at high subsonic Mach numbers. Hot-film measurements were conducted in study[7] in order to determine laminar, transitional, and turbulent boundary layer states. It was concluded that propeller-induced slipstream does not eliminate laminar separation bubble. Note that test conditions corresponded to Reynolds number of 5×10^5 and relatively low propeller's RPM.

The effect of a propeller slipstream on the wing laminar boundary layer was investigated[8] with the help of hot-wire sensors. Measurements in the boundary layer on the wing surface showed the periodic change of the laminar velocity profile to turbulent and back at the same rate as of the propeller rotation.

Additional references on the boundary layer transition as a function of a turbulence can be found elsewhere.[9] It is important to emphasize the fact that the previous studies[6-8] were performed for Reynolds numbers and thrust values relevant to large aircraft and high speed flights. Also, these studies were concerned with a rotational flow behind a single-propeller. Consequently, the results of the previous studies may or may not be applicable to the flow conditions pertaining to VTOL MAVs. Studies of slipstream disturbances and corresponding boundary layer flows characteristic to low Reynolds numbers free streams and slipstream induced by small propellers with high RPM are needed.

Since 2001, electric motors and lithium polymer batteries, especially those mass-produced for cellular phones, have become an enabling technology for MAVs.[10-12] The components of electric propulsion systems and guidelines for their evaluation and selection have been presented in detail for MAV applications.[13]

Effects of propulsive-induced flow on aerodynamic characteristics of MAVs in tractor configurations with a wing right behind a propeller have been studied experimentally.[14] A significant increase in lift coefficients (referred to a dynamic pressure in the free stream) and the delayed stall phenomenon was reported, especially when it comes to low-speed flight performance. The delayed stall seen with the induced propeller flow would allow a MAV to attain a higher angle of attack before aerodynamic stall, and hence attain a higher lift coefficient and slower flight speed than what would be thought possible just from wing aerodynamics alone. On the other hand, it was noticed that the lift-to-drag ratio for nearly all angles of attack are greater for the wing-only tests. It appears that even though the lift coefficients are increased due to the induced flow, the subsequent increase in the drag coefficient, both from the added lift and the parasite drag of the motor/propeller combination, increases the drag by a more substantial amount, leading to the decrease in the lift-to-drag ratios. To the contrary, investigations of a bi-plane configuration showed that the pusher arrangement of the propeller improves the overall performance of the vehicle.[15]

VTOL capabilities pose difficult problems for the fixed-wing MAV design. VTOL MAVs flying at low Reynolds numbers will have relatively large propeller sizes and larger control surfaces and throws. Owing to the complexity of the propeller-wing interactions, no design methods exist for sizing these airplanes. Therefore, in the present study, the aerodynamics of VTOL MAVs will be studied through wind tunnel measurements on the propulsion system consisting of two coaxial contra-rotating motors-propellers, wing, and wing-propeller combinations. As evident from the above discussion, the tilt-body concept with contra-rotating propellers represents a workable solution for the reduction or elimination of negative effects of other concepts. In the present study, a tilt-body VTOL MAV was designed based on previous successful designs.[3,4]

II. Models and Methods

A. Propulsion System for VTOL MAVs

The propulsion system shown in Fig. 1 consists of two pairs of coaxial contra-rotating motors and propellers. Each propeller is powered by a separate motor, rotating in opposite direction. This propulsion system was assembled by utilizing off-the-shelf brushless outrunners, MP Jet AC 22/4-60D.[16] The motors are joined at their stator backplates. The outrunner motors have a sufficient space inside the stators to allow a cross shaft through both motors, as shown in Fig. 1. The propeller 1 is attached to one end of the cross shaft and the other end is fixed to the rotor case of motor 1. The rotor of motor 2 was modified with an extended shaft, which also houses two bearings supporting the cross shaft. The motors have a diameter of 27 mm, and the total length of the propulsion is 60 mm. In this work, the motors are regulated by an electric speed controller, Phoenix-25, providing the same RPM (revolutions per minute) to both motors. The effect of unequal RPMs may be of interest for future studies, especially with regard to possible roll controlling of a vehicle through the differential RPMs.

Two arrangements of the propellers with respect to the motors were analyzed: tractor and pusher. In a tractor configuration, propellers are attached to the motors such that the thrust force is generated in the positive direction of the *s*-axis and the propeller slipstream hits the motors. For the pusher configuration, shown in Fig. 1, propellers were flipped 180° , and the polarity of the electric power was set to opposite. Propellers used are APC with a 140-mm diameter (radius R = 75 mm) and 114 mm-pitch. The distance between propellers is 17 mm.

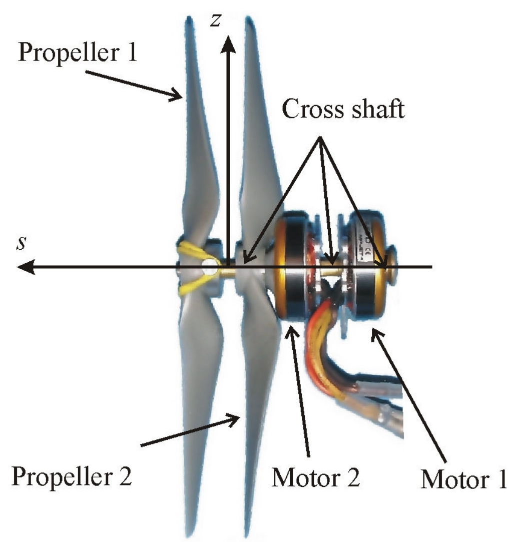

Fig. 1 Propulsion system of two coaxial contra-rotating motors-propellers.

B. Wing Design

The Zimmerman planform wing with a 254-mm wing span, 169-mm root chord, and aspect ratio of 1.91 is studied in this work. The S5010-TOP24C-REF airfoil[17] was utilized in designing the wing, with a maximum camber of 3% located at $0.24\,c$ and an inverse camber of 1% at $0.85\,c$. The wing geometry, presented in Fig. 2, was generated using SolidWorks™ as described in Ref. 18. It is stiffened by a plywood rib along the root chord, as shown in Fig. 3. The mold was manufactured employing 3D Printer InVision Si2. No fuselage or controls were attached to the wing studied in this work.

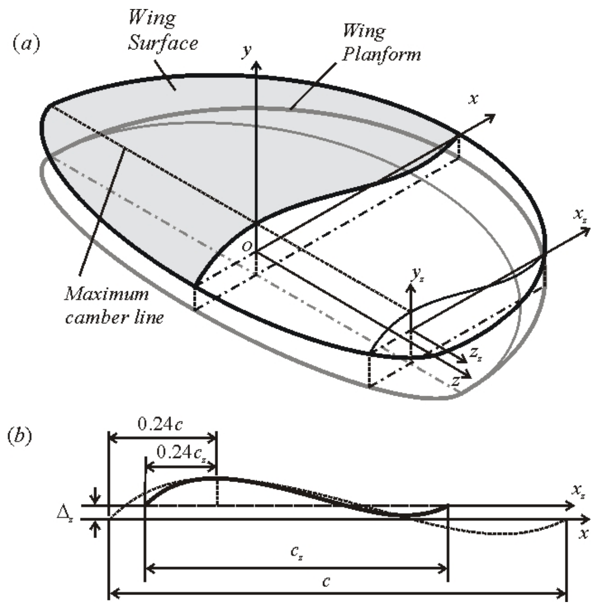

Fig. 2 Zimmerman wing (a) and representative cross section (b).

C. Motor Testing Bench and Hot-Wire Measuring System

The SUPAERO Propulsion Lab motor testing bench is used for the evaluation of small electric motor propulsion. It measures RPM, current, thrust and torque, with the voltage holding constant. Two load cells provide thrust and torque values. Calibration of the devices was done by applying a calibrated mass to the sensors. The resolution for the thrust force was 0.005 N and for the torque 0.2 N mm.

A hot-wire measuring system has been used to investigate the velocity profile of propeller flow. The sensor is a 2D hot-wire, Model 1241-20 from TSI. It allows two normal velocity components to be measured, but in this study only axial flow velocity was used. This sensor is managed by an IFA 300 constant- temperature anemometer system from TSI. The two electric signals resulting from this acquisition system are translated into two velocity values using a MATLAB routine on the acquisition computer. Calibration of the acquisition system is achieved in the wind tunnel test section. A 2D map of each wire voltage is generated using wind speed and sensor angle as the two input parameters. Discreet values of wind speed from 0 to 30 m/s are set with a step of 1 m/s. For each wind speed, the sensor angle is set from -45° to 45°, with a 1° step. The resulting 2D map for one wire is a continuous surface. A voltage value for this wire will result in a line in the (wind speed, angle) plane. Given a voltage for each wire, the intersection of the resulting lines will lead to a single point equivalent to unique speed and angle values. This calibration method provides better accuracy for the whole measurement range than the usual polynomial formula. The wind speed measured during calibration is provided from a calibrated Pitot tube, whose accuracy is better than 0.1 m/s for the speed range obtained from the propeller flow. The angle is measured by a digital potentiometer, which has a precision of 0.01°.

Experimental arrangements for testing a wing with a motor is presented in Fig. 3. For testing of the motor only, the wing was removed and testing was conducted using the same fixture.

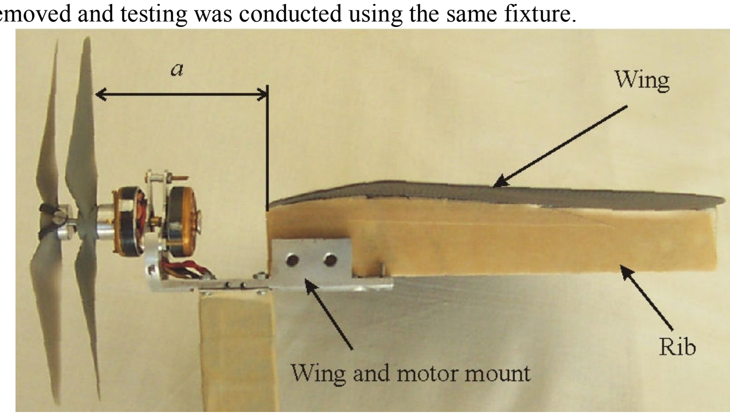

Fig. 3 Experimental arrangements for testing of a wing with a motor.

D. Wind Tunnel Facility

The SUPAERO low-speed wind tunnel is a closed-loop wind tunnel where test section has a 0.45×0.45 m cross section and is 0.7 m long. The contraction ratio is 6.2 and the turbulence level is 1%. Speeds from 2 m/s to 30 m/s can be obtained with a standard deviation below 0.2 m/s.

The balance measures all the aerodynamic components except for the side force. It is composed of 6 single-ended load cells. Three struts, each linked to 2 cells, go through the test section floor and connect to the test model. Balance calibration is achieved by computing the calibration slope of each cell using calibrated weights. The resolution for forces is less than 0.004 N.

A calibration of the wind tunnel and the balance was performed before each test series. Utilizing calibration measurements and the small-sample method,[19] the uncertainty intervals in aerodynamic coefficients were determined. Standard deviations of aerodynamic coefficients were estimated. Solid blockage, wake blockage, and streamlined curvature corrections were estimated based on the methods described in Ref. 20.

III. Evaluation of Propulsion System

A. Motor Static Testing

The performance in hover and vertical climb of a VTOL aircraft is a driving factor in the take-off weight determination and power selection. Since these flight conditions are characterized by a relatively low speed, knowledge of the static thrust at zero free stream velocity becomes very important. Other parameters affecting the design include torque, RPM, and power requirements. Several propulsion systems were evaluated on the motor testing bench. The tests were conducted for a constant voltage from 6 to 11 V, with a step of 0.5 V. With the voltage set, the motor(s) was started and measurements were taken at the control signal to the motors in terms of PWM (pulse width modulation) varied from 50% to 80%, where the former corresponds to 1.5 ms and latter to 1.8 ms. Both tractor and pusher arrangements of contra-rotating propulsion were investigated, as well as a conventional single motor-propeller setup.

In Fig. 4, the variation of thrust and torque with PWM is presented for the tractor at 11 V. The thrust force increases linearly with PWM and reaches a maximum at 3.42 N and at 12,000 RPM. This thrust is 1.9 greater than the thrust generated by a single propeller-motor under the same voltage and PWM. Thus, there is a small loss of the thrust in the contra-rotating system compared to a single propeller-motor, which can be explained by the non-optimal propellers selected for the present study. Note that the linear relationship simplifies thrust control in an automatic system.

The maximum torque in this test was 0.42 N cm, which is also the maximum torque measured in all tests conducted for contra-rotating systems. As expected, this torque was about 10 times lower in comparison with a torque measured on a single propeller-motor system. This feature of the contra-rotating propulsion significantly simplifies controls for VTOL aircraft, and it is a major advantage of the presented propulsion system.

Figure 5 shows static thrust generated by both pusher and tractor propulsion systems as a function of electric power input. The presented data provide estimates of the power required for hovering flight and can be used for battery selection. As evident from Fig. 5, the pusher propulsion generates 20-23% more thrust force than the tractor for the same inputted power. It directly affects the take-off weight and flight performance of the vehicle in hover and climb. In the tractor configuration, the motor is placed right behind propellers and, therefore, creates a significant parasite drag. Hence, the shape optimization of the motor mount and fuselage is another important area of research for aerodynamic design at low Reynolds numbers.

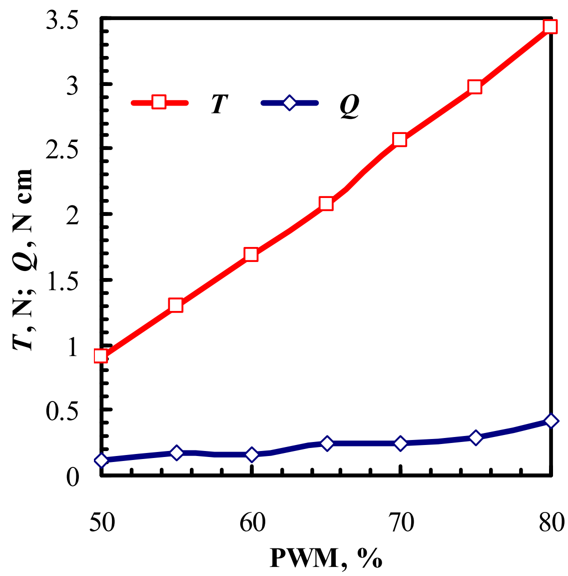

Fig. 4 Variation of thrust and torque with PWM (pulse width modulation).

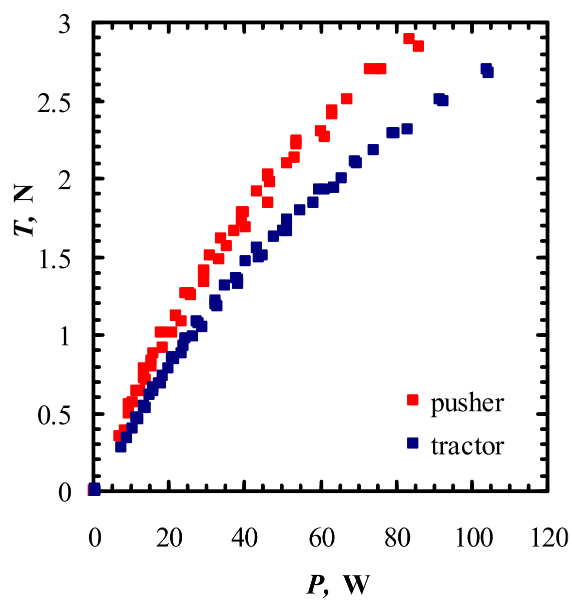

Fig. 5 Thrust of propulsion system as a function of input power.

B. Slipstream Velocity Profiles

A hot-wire system was utilized for measuring air velocity profiles in a slipstream behind the propellers. While a propulsion system was still sitting on the motor testing bench, the hot-wire probe was mounted on its top, allowing simultaneous measurements of air velocity and thrust, power input, voltage, etc. The testing was conducted at constant voltage of 8.5 V and the PWM was set to hold the thrust constant. However, in the course of the tests, a 3-5 % drift of the thrust has been observed and PWM was manually adjusted to the desired thrust.

The measurements were conducted at four sections located at distances, s = 35, 70, 130, and -70 mm (Fig. 1), respectively, with the first three sections referring to the pusher arrangement, while the last section refers to the tractor. For each section, the air velocity component in the s-direction was measured at points along the z-coordinate distant from the motor-propeller axis from 0 to a maximum distance $R_m = 85$ mm, with a step of 1 mm. The propeller's radius R corresponds to $z = 75$ mm.

Air velocity distribution in the pusher propeller slipstream can be seen in Fig. 6 for two values of thrust: T = 1.47 N and T = 2.45 N. The plots exhibit a single-hump shape, with the maximum of velocity near the point $z = 0.5R$. With z increases beyond the propeller radius, the velocity asymptotically approaches zero. The local decrease of the air velocity (by about 15%) closer to the axis of rotation may be caused by the propeller's hub and the interference of the propellers with the motors. The fluctuations in velocities in terms of a standard deviation were determined and error bars plotted in Fig. 6. They are indicative of non-stationary, pulsating flow behind the propellers. The increase in size of the error bar illustrates the presence of vortices in the area near the propeller tips. Also, larger pulsations are noticed for higher thrust force.

Air velocity profiles in Fig. 7 are shown for three sections at the same thrust force. This figure shows the change in the profile: the farther they are from the propeller, the more uniform they become.

Figure 8 illustrates velocity profiles at sections placed at the same distance, $|s| = 70$ mm, from the propeller in the pusher and tractor arrangements. In fact, for the tractor arrangement, the velocity is measured right behind the aft motor. The lower average velocity and significant decrease of velocity in the core of the slipstream found in tractor arrangement are mostly due to the parasite drag caused by the motors and to some degree by the motor mount. These results also explain the overall decrease of the thrust force for the tractor arrangement in comparison with the pusher one, as evident from Fig. 5.

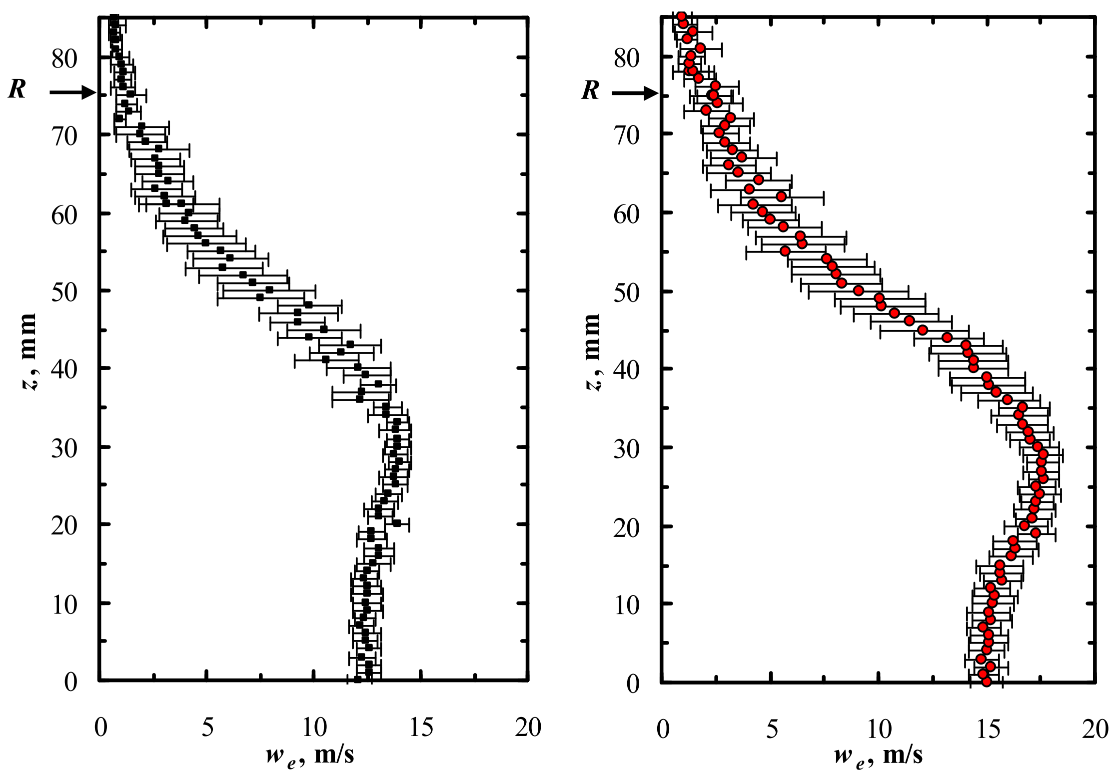

Fig. 6 Experimental velocity profiles at section s =130 mm at T = 1.47 N (left) and T = 2.45 N (right) for a pusher arrangement.

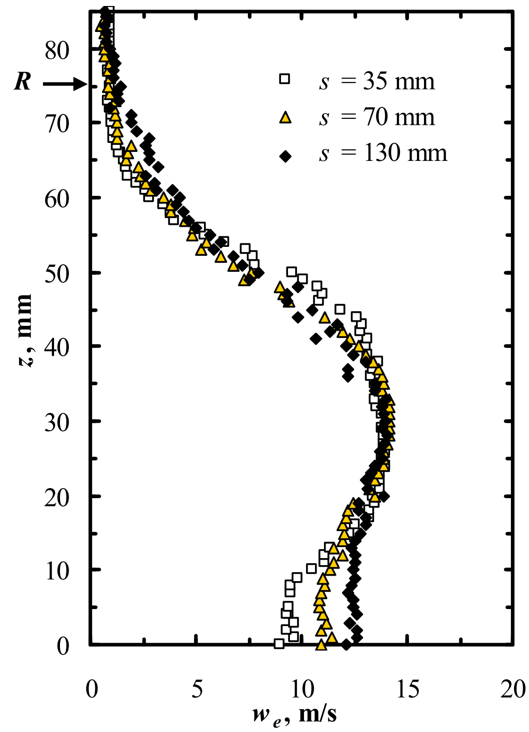

Fig. 7   Comparison of air velocity profiles for three sections in a pusher at *T* = 1.47 N.

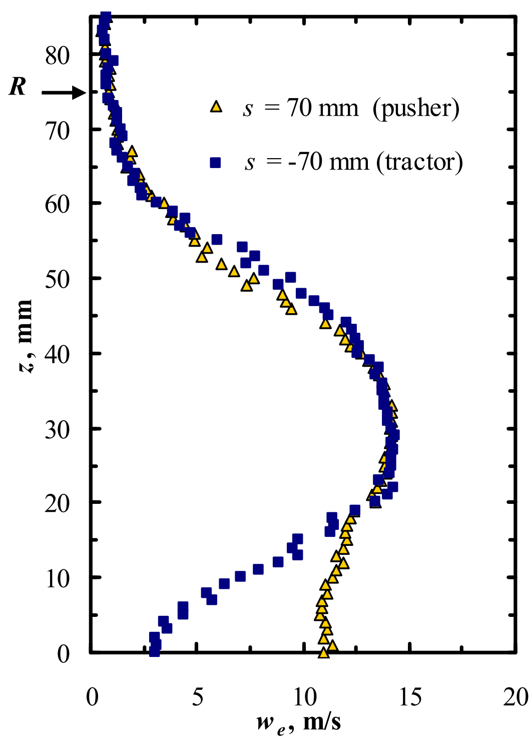

Fig. 8   Pusher vs tractor comparisons for air velocity profiles at *s* = 70 mm and -70 mm, *T* = 1.47 N.

Now, utilizing measured air velocity data, the values of thrust and induced power can be determined. Consider a cylindrical control volume around the propeller. It is assumed to be very large so that the transport of mass and momentum through its walls is negligible, except through the side circular wall of radius $R_m = 85$ mm (of area, S_S) placed in the propeller slipstream at a distance s from the propeller. Applying the momentum and energy theorems, the static thrust is found from

$$T_s = \rho \int_{S_S} V^2 dS \tag{1}$$

while the power induced into the flow is

$$P_{ind} = \frac{\rho}{2} \int_{S_S} V^3 dS \tag{2}$$

Assuming that the air velocity remains constant in the azimuthal direction, the calculations of T_s and P_{ind} were conducted by substituting hot-wire data into Eq. (1) and (2). In addition, the figure of merit, $f_M = P_{ind} / P$, was computed.

Numerical results obtained through the use of air velocity data for sections $s = 70$ mm (for pusher) and $s = -70$ mm (for tractor) are presented in Table 1 for the nominal thrust of 1.47 N. Obtained T_s values differ from the nominal by about 5%, which is a good agreement when one takes into account the drift (mentioned above) of the thrust during these tests. As expected, for the same nominal thrust, the pusher generates higher induced power and has a higher figure of merit.

Table 1. Thrust, power, and figure of merit for propulsion systems.

Propeller Arrangement	T_s (N)	P (W)	P_{ind} (W)	f_M
Pusher	1.43	42.5	8.62	0.20
Tractor	1.55	45.0	8.20	0.18

The obtained results will be used here for verification of the propeller momentum theory for slipstream velocity predictions. By following derivations from Ref. 1, the propeller-induced velocity at the distance s from the propeller disk is given by

$$w(s) = 0.5\left[\sqrt{V_0^2 + \frac{2T}{\rho \pi R^2}}\left(1 + \frac{s/R}{\sqrt{1+(s/R)^2}}\right) - V_0\right] \tag{3}$$

where V_0 is a free stream velocity in front of the propeller. The radius of the stream tube induced by the propeller, r, can be found from the continuity equation

$$w(s) r^2 = w(0) R^2 \tag{4}$$

The velocity and the radius of the stream tube were calculated for the section $s = 70$ mm for two values of the static thrust. The numerical results obtained with the help of Eq. (3) are shown in Fig. 9, together with experimental data, w_e. Overall, their matching is good and, therefore, the propeller momentum theory can be recommended for air velocity predictions to be used in the aerodynamic analysis and sizing of the wing, fuselage, and control surfaces of VTOL MAVs.

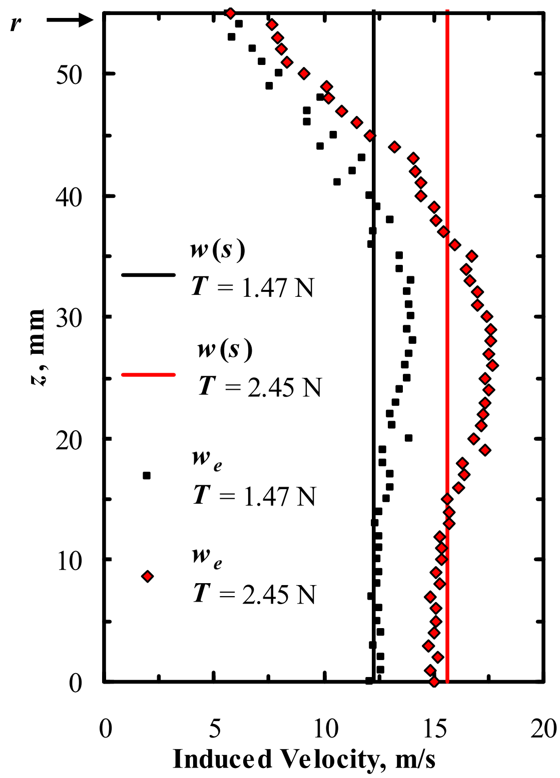

Fig. 9 Comparison of experimental results against propeller momentum theory at s = 70 mm.

IV. Wind Tunnel Testing

A. Wing Only Tests

Experimental measurements in wind tunnels at low Reynolds numbers become difficult because aerodynamic forces are small at low angles of attack, requiring high accuracy and sensitivity of measuring facilities. For these reasons, the validation of available aerodynamic data for wings used in the current designs is an important task itself in the development of a reliable database on MAVs.

A series of wind tunnel tests was conducted on wind tunnel models of the Zimmerman wing with 3 and 9 % camber.[18] These tests were done without a motor or fuselage in order to determine the exact role that camber plays in the aerodynamics of the vehicles. In the present study, the same 3% model that was previously tested in the University of Arizona wind tunnel[18] was tested in SUPAERO wind tunnel.

The tests were conducted for two values of the Reynolds numbers, 5×10^4 and 10^5, and the results are presented in Figs. 10 and 11 for the lift and drag coefficients, respectively. It can be seen from the plots that lift coefficients are in reasonable agreement for both high and low angles of attack. For the drag coefficients, there is a reasonable agreement of the results at the moderate angles of attack, which becomes worse when α approaches angles corresponding to the maximum lift coefficient.

The zero-lift drag coefficient, C_{D_0}, is especially interesting in designing MAVs for hovering and vertical flight conditions. For the Reynolds number 10^5, the C_{D_0} coefficient obtained in SUAPERO is 0.025, which is higher than the value of 0.02 from the UA tests. Note that for very small α, the magnitude of the measured drag becomes smaller and it has increased scatter for both testing facilities.

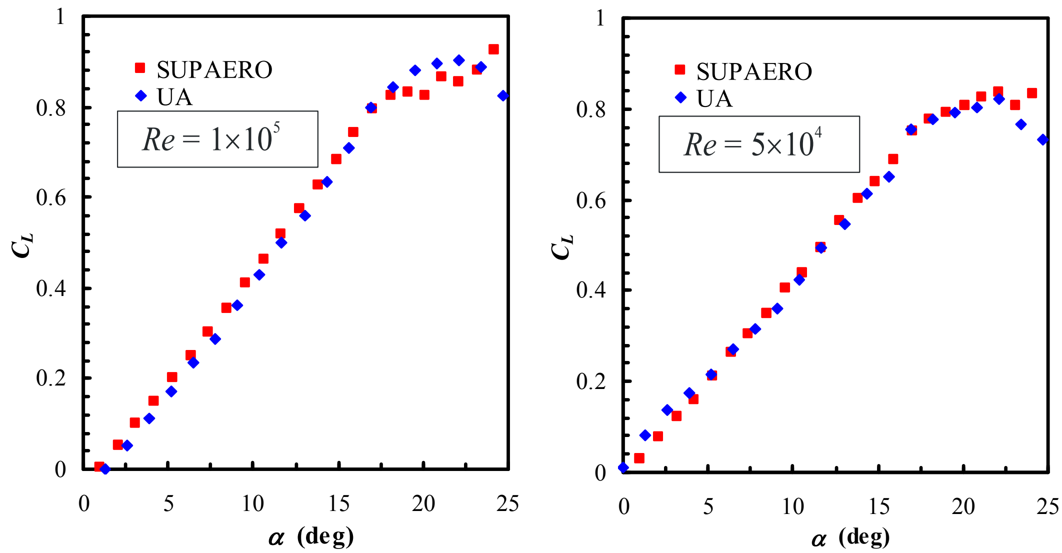

Fig. 10 Lift coefficient variation with angle of attack.

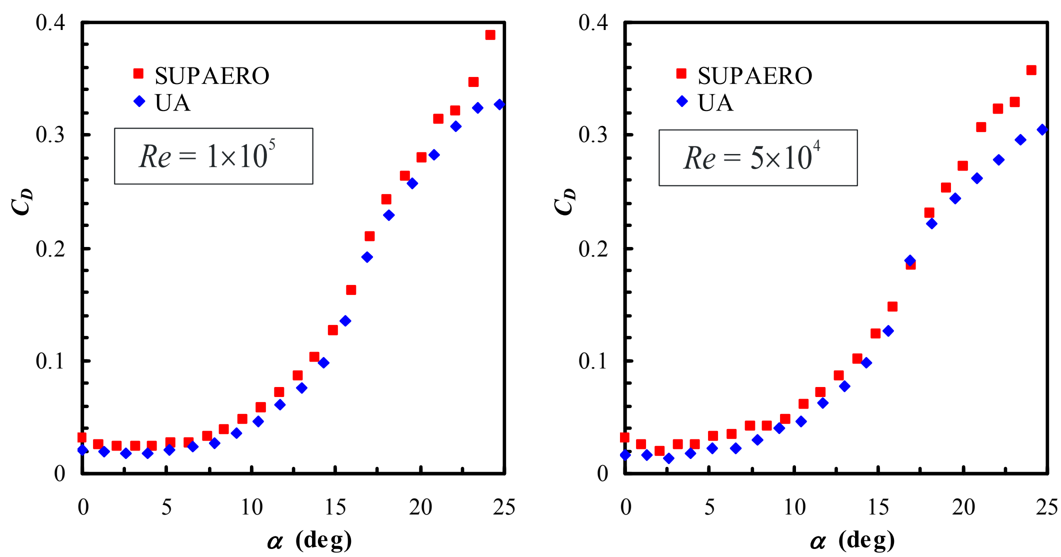

Fig. 11 Drag coefficient variation with angle of attack.

B. Motor Tests in Wind Tunnel

The contra-rotating propulsion system in a tractor arrangement was mounted to the top of the struts in the SUPAERO wind tunnel test section, and an electrical connection was established between the motor and a power supply located outside of the wind tunnel. With the power set to on and the motor running, the tunnel flow was started and thrust measurements were taken at tunnel velocities ranging from 0 to 15 m/s. The tests were conducted with 11 V supplied to the motors and with PWM varying from 55 to 70 %, so an accurate model of the thrust behavior of the propulsion was obtained. A difference between the test-bench and wind tunnel static thrust data was noticed that can be attributed to the different drags of the struts on the test-bench and in the wind tunnel.

The experimental results are presented in Fig. 12 for PWM = 55, 60, 65, and 70 %, and, as expected, the thrust decreases as free stream velocity increases.

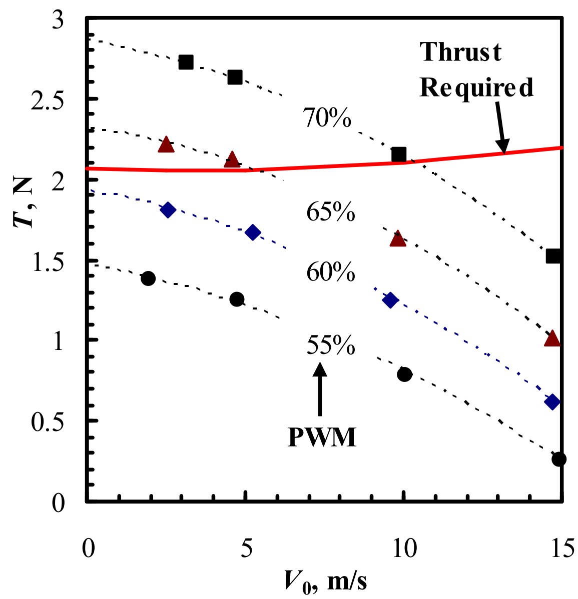

Fig. 12 Thrust available and required variations with free stream speed (symbols – experimental data points, dashed lines – quadratic approximations).

C. Determination of Wing Drag due to Free Stream and Propeller Slipstream

Hover and vertical flight efficiency is one of the single-most important qualities that VTOL MAVs must exhibit. It affects the maximum required thrust and power and determines the endurance for loitering over a target area. This part of the study will focus on the determination of drag forces at near-zero angles of attack in the presence of both free stream flow and propeller-induced flow.

This series of tests was conducted in the SUPAERO wind tunnel. The wind tunnel model shown in Fig. 3 consists of the contra-rotating propulsion and Zimmerman wing connected through a common mount fixture. The motor was installed such that the thrust line is collinear with the root chord line.

The motor was set at 11 V and PWM varied from 55 to 70%. The free stream velocity, V_0, ranges from 0 to 15 m/sec. For a given combination of PWM and V_0, the wind tunnel balance measures a total force, F_{total}, which is the sum of the thrust force generated by a propeller and the drag force on the wing. This force corresponds to a zero-lift angle of attack. From the motor tests described in the previous section, the amount of thrust, T, produced at each free stream velocity, V_0, is known. The drag on the wing, D_0, is generated from two mixing airflows: free stream and propeller slipstream. Since the motor and wing were mounted on the same fixture as in the motor only tests, the drag force can be determined as $D_0 = |F_{total} - T|$ and is presented in Fig. 13. For clarification, the total force, F_{total}, is smaller in magnitude than the propulsive thrust, T, and also because of the test procedure, the zero-lift drag force D_0 has no fixture or strut effects on it.

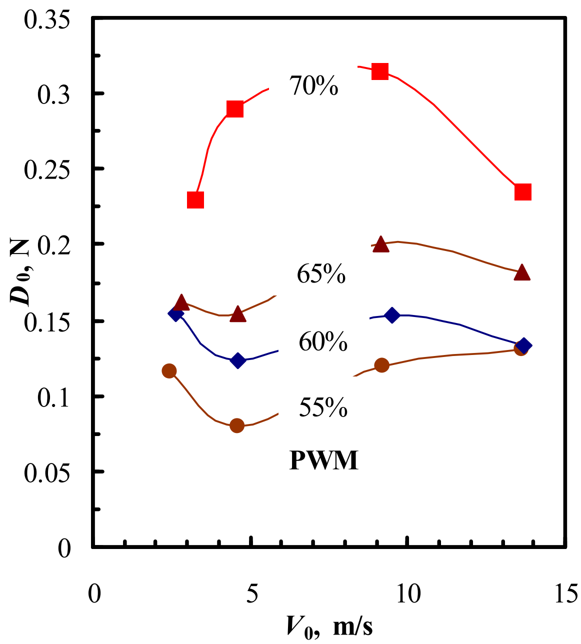

Fig. 13 Drag on the wing due to propeller slipstream and free stream.

Consider the air flow over the wing. We introduce a simplified model for the flow similar to the one used in the classical propeller momentum theory.[1] The free stream V_0 enters the propeller and wing, Fig. 14. Assume that a cylindrical stream tube is formed behind the propeller of a diameter equal to the propeller's diameter, $2R$. The second assumption is that velocity induced by a propeller is constant along the stream tube and is equal in magnitude to its ultimate value derived in the momentum theory, which is

$$w_{ult} = w(s=\infty) = \sqrt{V_0^2 + \frac{2T}{\rho \pi R^2}} - V_0 \tag{5}$$

and the velocity behind the propeller disk is a sum

$$V_0 + w_{ult} = \sqrt{V_0^2 + \frac{2T}{\rho \pi R^2}} \tag{6}$$

The zero-lift drag produced by the wing body can be presented as

$$D_0 = 0.5 \rho C_{D_0} \left[S_0 \left(V_0 + w_{ult} \right)^2 + \left(S_0 - S_p \right) V_0^2 \right] \tag{7}$$

where S_p is the area of a part of the wing covered by the propeller slipstream and is shown in Fig. 14. Through division, we arrive at the zero-lift drag coefficient in the presence of a free stream and slipstream

$$C_{D_0} = \frac{D_0}{0.5 \rho \left[S_0 \left(V_0 + w_{ult} \right)^2 + \left(S_0 - S_p \right) V_0^2 \right]} \tag{8}$$

This formula is valid also for either propeller-induced velocity or free stream velocity to be zero.

Using obtained experimental data for drag force, the drag coefficients C_{D_0} were computed from Eq. (8) as a function of the ultimate induced velocity, w_{ult}, computed by Eq. (5) and the results are presented in Fig. 15.

They clearly demonstrate that the slipstream behind the propeller has a profound negative effect on the drag of the wing.

For a low power and low w_{ult} conditions, the wing drag coefficient approaches the value for laminar flow (0.02-0.025) obtained for the wing-only test. The drag coefficient increases by about three times, with induced speed increasing from 0 to 15 m/sec. This result indicates the change of transition mechanism in the boundary layer from a laminar to turbulent state, which deserves further study.

Although the data are scattered, the correlation between drag coefficient and induced velocity is meaningful and can be approximated by the linear equation

$$C_{D_0} = 0.0305 + 0.0024 w_{ult} \tag{9}$$

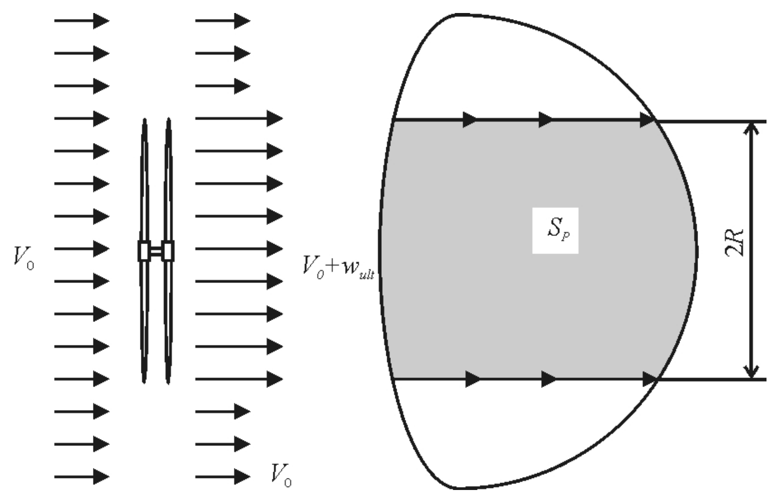

Fig. 14 Model of flow velocity over the wing.

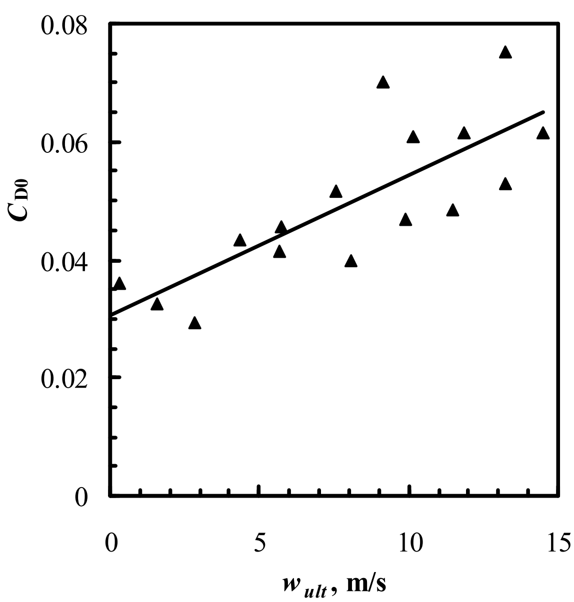

Fig. 15 Zero-lift drag coefficient variation with ultimate induced velocity.

V. Designing VTOL MAV Prototype

The obtained results can be used for designing VTOL MAVs with vertical flight requirements. Even though this procedure gives only one design point, it is an utmost important one for the selection of propulsion system and power source. For the steady vertical flight of the aircraft with a take-off weight of W, the balance of forces in a vertical direction can be written as

$$T - W - D_0 = 0 \tag{10}$$

By combining Eq. (5), (7), (9), and (10), the thrust required for the vertical flight at a speed V_0 can be found from

$$T - W + 0.5\rho\left[0.0305 + 0.0024\left(\sqrt{V_0^2 + \frac{2T}{\rho\pi R^2}} - V_0^2\right)\right]\left[S_0\left(V_0^2 + \frac{2T}{\rho\pi R^2}\right) + \left(S_0 - S_p\right)V_0^2\right] = 0 \tag{11}$$

The first VTOL MAV prototype (Fig. 16) has been designed based on the propulsion system described in this paper. The aircraft is equipped with a flat plate wing of Zimmerman planform. It has a take-off weight of $W = 1.76$ N, wingspan of 30 cm, wing area of $S_0 = 335$ cm^2, and an area of the wing portion covered by the propeller slipstream $S_p = 210$ cm^2. Using these data, the thrust required to climb vertically with a rate-of-climb V_0 was obtained numerically from Eq. (11) and plotted in Fig. 12. It can be seen that with the rate-of-climb increases, the required thrust is slightly increased with a maximum of 2.3 N. From comparison of thrust available and required (Fig. 12), the thrust available from the current propulsion will provide a steady vertical flight in the range of climb-rates 0-10 m/s, with PWM in the range of 62-70%.

As can be seen from Fig. 5, about 80 W of maximum power is needed to support the flight mission characterized by the maximum required thrust of 2.3 N. To satisfy this requirement, a 3-cell lithium-polymer battery, of 740 mAh capacity, was selected as an onboard power source.

Two fins with a total area of 47 cm^2 provide the stabilization of the aircraft in roll and yaw. A rudder consisting of two connected sections of a total area of 30 cm^2 is attached to fins. Two elevons of total area 60 cm^2 control the vehicle in pitch and yaw. Test flights were conducted with this vehicle demonstrating a hover, sustained vertical climbs, and transition to and from a level flight.

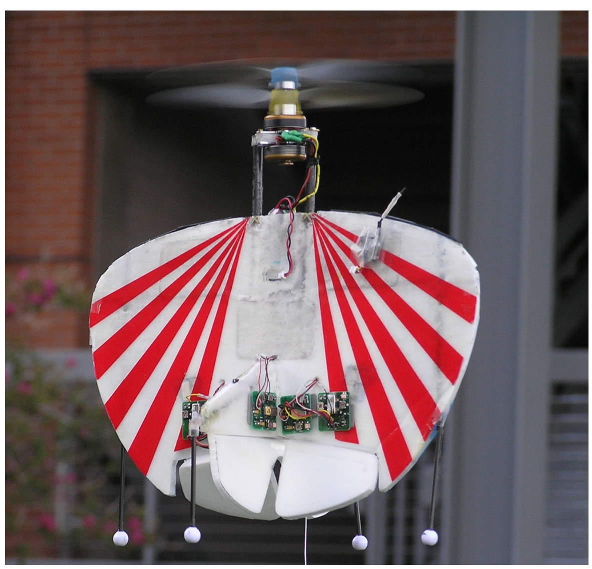

Fig. 16 VTOL MAV in flight.

VI. Conclusions

In the present study, a tilt-body, tail-sitter concept for VTOL MAVs was analyzed and a novel design was proposed based on the contra-rotating propeller-motor electric propulsion system. As evident from the discussion, this design represents a workable solution for the reduction or elimination of the negative effects of other concepts.

The evaluation of the propulsion was conducted for two propeller arrangements: pusher and tractor. Static thrust measurements, as well as RPM, power, and torque, were conducted on a motor testing bench. A small loss of thrust in the contra-rotating system was found compared to a single propeller-motor. The maximum torque for the contra-rotating system was about 10 times lower than a torque measured on a single propeller-motor system. The pusher arrangement of the propeller generates 20-23% more thrust force than the tractor for the same inputted power. In the tractor configuration, the motor is placed right behind the propellers, creating a significant parasite drag. Hence, the shape optimization of a motor mount and fuselage is another important area of research for aerodynamic design at low Reynolds numbers.

A hot-wire system was utilized for measuring air velocity profiles in a slipstream behind propellers. The fluctuations in velocities in terms of a standard deviation were determined. They are indicative of non-stationary, pulsating flow behind the propellers. For the tractor arrangement, lower average velocity and a significant decrease of velocity in the slipstream core are mostly due to the parasite drag caused by the motors' placement right behind the propellers. These results also explain the overall decrease of a thrust force for the tractor arrangement in comparison with the pusher one.

In the present study, the same 3% Zimmerman wing that was previously tested in the University of Arizona wind tunnel was tested in the SUPAERO wind tunnel. The results for the lift and drag coefficients are in reasonable agreement for both high and low angles of attack.

The aerodynamics of a wing-propeller combination was studied through wind tunnel measurements. Results clearly demonstrate that for a given range of propeller thrust, the slipstream behind the propeller has a profound negative effect on the drag of the wing for zero-lift angles of attack. The drag on the wing is generated from two mixing airflows: free stream and propeller slipstream. A simplified model for the flow similar to the one used in the classical propeller momentum theory is introduced in the present study, and a formula for the drag coefficient for the wing in the presence of a free stream and slipstream is derived.

Using obtained experimental data for drag forces, the zero-lift drag coefficients were computed as a function of the ultimate induced velocity. The drag coefficient increases three times, with induced speed increasing from 0 to 15 m/sec. This result indicates the change of transition mechanism in the boundary layer from a laminar to a turbulent state, which deserves further study.

The results obtained in the present study were realized in a design of a VTOL MAV prototype that was successfully flight tested.

Acknowledgments

This project represents collaborative efforts of the University of Arizona and SUPAERO towards the development of VTOL MAV technologies. It was sponsored by grants from the AFRL, Eglin AFB (Program Manager Dr. Gregg Abate), to the University of Arizona and by EOARD, London (Program Manager Dr. Surya Surampudi), to the SUPAERO. The authors also would like to thank the other members of the Micro Air Vehicle Project at both universities for their contributions to this work: Bill Silin, David Addai, and Chinnapat Thipyopas. S. Shkarayev would like to thank the SUPAERO team for their support of research on VTOL MAVs during his visiting appointment there.

References

[1]McCormick, B. W. Jr., *Aerodynamics of V/STOL Flight*, Dover Publications, Inc., Mineola, NY, 1999.

[2]Kohlman, D., *Introduction to V/STOL Airplanes,* Iowa State University Press, Ames, IA, 1981.

[3]Krashanitsa, R., Platanitis, G., Silin, D., and Shkarayev, S., "Autopilot Integration into Micro Air Vehicles," Chapter 3, *Introduction to the Design of Fixed-Wing Micro Aerial Vehicles,* edited by T. J. Mueller, J. C. Kellogg, P. G. Ifju, and S. V. Shkarayev, AIAA, Reston, VA, 2007, pp. 109-149.

[4]Bataille, B., Poinsot, D., Thipyopas, C., and Moschetta, J.M., "Fixed-Wing Micro Air Vehicles with Hovering Capabilities," NATO RTO meeting, AVT-146, Symposium on "Platform Innovations and System Integration for Unmanned Air, Land and Sea Vehicles," Florence, Italy, May 14-17, 2007.

[5]Prandtl, L., "Mutual Influence of Wings and Propeller," NACA TN 74, Extract from *The First Report of the Gottingen Aerodynamic Laboratory*, Chapter IV, Sec. 6, December, 1921.

[6]Hood, M. J., and Gaydos, M. E., "Effects of Propellers and Vibration on the Extent of Laminar Flow on the NACA 27-212 Airfoil," NACA ACR (WR L-784), 1939.

[7]Elsaadawy, E. A., and Britcher, C. P. "Effect of Propeller Slipstream on Heat-Exchanger Installations at Low Reynolds Number," *J. Aircraft*, Vol. 40, 2003, pp. 751-758.

[8]Miley, S. J., Howard, R. M., and Holmes, B. J., "Wing Laminar Boundary Layer in the Presence of a Propeller Slipstream," *J. Aircraft*, Vol. 25, 1988, pp. 606-611.

[9]Hoerner, S. F., *Fluid-Dynamic Drag*, Hoerner Fluid Dynamics, Bakersfield, CA, 1965.

[10]Micro Air Vehicle Design Papers, 6th International MAV Competition, Brigham Young University, Provo, UT, April 2002.

[11]Micro Air Vehicle Design Papers, 7th International MAV Competition, University of Florida, Gainesville, FL, April 2003.

[12]Micro Air Vehicle Design Papers, 8th international MAV Competition, The University of Arizona, Tucson, AZ, April 2004.

[13]Mueller, T. J., Torres, G. E., Srull, D. W., Elements of Aerodynamics, Propulsion, and Design, Chapter 2, *Introduction to the Design of Fixed-Wing Micro Aerial Vehicles,* Edited by J. Mueller, J. C. Kellogg, P. G. Ifju, and S. V. Shkarayev, AIAA, Reston, VA, 2006, pp. 39-107.

[14]Null, W., Noseck, A., and Shkarayev, S., "Effects of Propulsive-Induced Flow on the Aerodynamics of Micro Air Vehicles," 23rd AIAA Applied Aerodynamics Conference, AIAA 2005-4626, Toronto, Canada, 2005.

[15]Moschetta J. M. and Thipyopas C., "Aerodynamic Performance of a Biplane Micro Air Vehicle," *Journal of Aircraft*, Vol. 44, 2007, pp. 291-299.

[16]MP Jet Electromotor AC 22/4-60 D, MP Jet, Rudolfovska 87, P.O. BOX 100, CZ -370 21 C. Budejovice, Czech Republic, 2007.

[17]Null, W. and Shkarayev, S., "Effect of Camber on the Aerodynamics of Adaptive Wing Micro Air Vehicles," *J. Aircraft*, Vol. 42, 2005, pp. 1537-1542.

[18]Aki, M., Waszak, M., and Shkarayev, S., "Development of Micro Air Vehicles with In-Flight Adaptive Wing," Chapter 6, *Introduction to the Design of Fixed-Wing Micro Aerial Vehicles*, Edited by J. Mueller, J. C. Kellogg, P. G. Ifju, and S. V. Shkarayev, AIAA, Reston, VA, 2006, pp. 241-275.

[19]Kline, S. J., and McClintock, F. A., "Describing Uncertainties in Single-Sample Experiments," *Mech Eng*, Vol. 75, No.1, 1953, pp. 3-8.

[20]Barlow, J. B., Rae, W. H., Jr., and Pope, A., *Low-Speed Wind Tunnel Testing*, 3rd Ed., Wiley, New York, 1999.